

MeanFuser: Fast One-Step Multi-Modal Trajectory Generation and Adaptive Reconstruction via MeanFlow for End-to-End Autonomous Driving

Junli Wang^{1,2,3*}, Xueyi Liu^{1,2}, Zebin Xing^{1,2}, Yinan Zheng^{3,4}, Pengfei Li⁴, Guang Li³, Kun Ma³, Guang Chen³, Hangjun Ye³, Zhongpu Xia^{1,2}, Long Chen³, Qichao Zhang^{1,2†}

¹ SKL-MAIS, Institute of Automation, Chinese Academy of Sciences

² School of Artificial Intelligence, University of Chinese Academy of Sciences

³ Xiaomi EV ⁴ Institute for AI Industry Research (AIR), Tsinghua University

Abstract

Generative models have shown great potential in trajectory planning. Recent studies demonstrate that anchor-guided generative models are effective in modeling the uncertainty of driving behaviors and improving overall performance. However, these methods rely on discrete anchor vocabularies that must sufficiently cover the trajectory distribution during testing to ensure robustness, inducing an inherent trade-off between vocabulary size and model performance. To overcome this limitation, we propose **MeanFuser**, an end-to-end autonomous driving method that enhances both efficiency and robustness through three key designs. (1) We introduce Gaussian Mixture Noise (GMN) to guide generative sampling, enabling a continuous representation of the trajectory space and eliminating the dependency on discrete anchor vocabularies. (2) We adapt “MeanFlow Identity” to end-to-end planning, which models the mean velocity field between GMN and trajectory distribution instead of the instantaneous velocity field used in vanilla flow matching methods, effectively eliminating numerical errors from ODE solvers and significantly accelerating inference. (3) We design a lightweight Adaptive Reconstruction Module (ARM) that enables the model to implicitly select from all sampled proposals or reconstruct a new trajectory when none is satisfactory via attention weights. Experiments on the NAVSIM closed-loop benchmark demonstrate that MeanFuser achieves outstanding performance without the supervision of the PDM Score. and exceptional inference efficiency, offering a robust and efficient solution for end-to-end autonomous driving. Our code and model are available at <https://github.com/wjl2244/MeanFuser>.

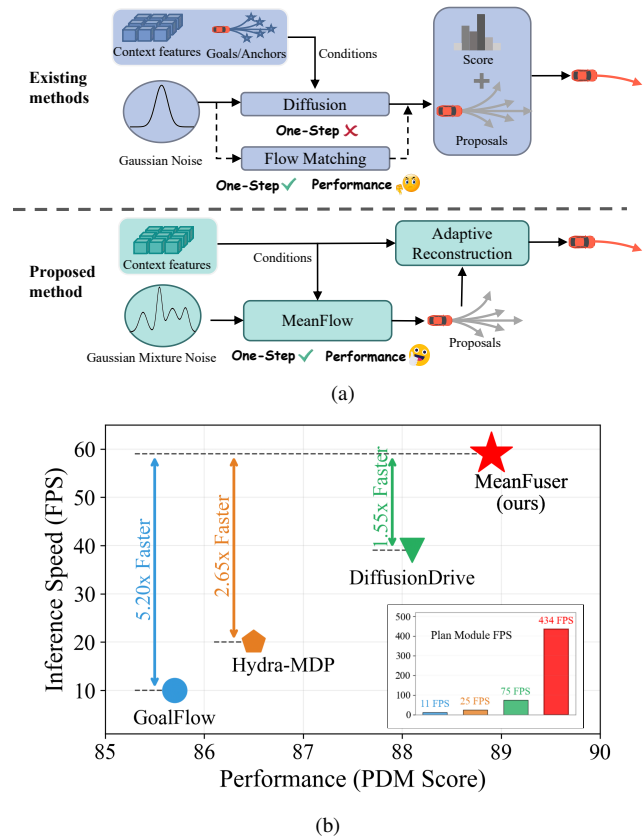


Figure 1. (a) illustrates the differences between our proposed method and existing generative approaches, highlighting the introduction of Gaussian mixture noise to replace anchor vocabularies, one-step sampling, and the adaptive reconstruction module. (b) shows the advantages of MeanFuser over GoalFlow[31], Hydra-MDP[17], and DiffusionDrive[19] in terms of closed-loop performance, inference speed and plan module inference speed.

* Completed during internship at Xiaomi EV. † Corresponding author

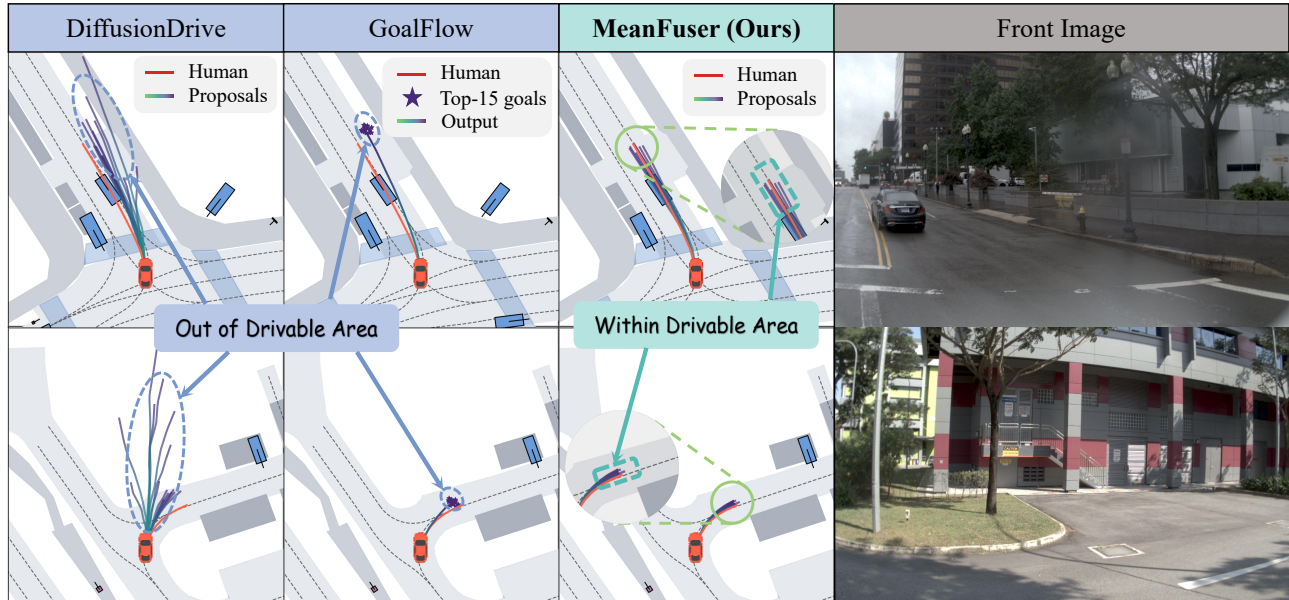


Figure 2. Failure scene visualization. Anchor-guided models (GoalFlow, DiffusionDrive) fail due to the inability of discrete vocabularies to cover the entire trajectory space, while our model generates proposals that encompass the optimal trajectories.

1. Introduction

End-to-end autonomous driving[2, 5, 11–13, 19, 22, 30, 36] has attracted considerable attention as it directly learns the mapping from raw sensor inputs to planned trajectories, thereby avoiding handcrafted rules in rule-based systems and the cumulative errors inherent in modular pipelines.

High-performance frameworks such as TransFuser[5], UniAD[12], and VAD[13] have demonstrated impressive driving capabilities by learning unimodal trajectories. However, they fail to effectively capture the multi-modal nature and uncertainty of driving behaviors. Methods like VADv2[3] and Hydra-MDP[17] introduce a trajectory vocabulary and predict the probability distribution of each trajectory under specific scenarios. However, a fixed vocabulary size imposes a trade-off between efficiency and robustness. Large vocabularies slow down inference, while small ones tend to fail under distribution shifts.

Recently, generative models such as diffusion models[10, 24, 25] and flow-based models[9, 20, 21] have demonstrated remarkable capabilities in capturing complex data distributions, leading to significant breakthroughs in fields like image generation and robot learning[4, 23, 35]. Motivated by their success, researchers have begun exploring the use of diffusion and flow matching frameworks in end-to-end autonomous driving. However, vanilla diffusion models often suffer from mode collapse[6], resulting in limited trajectory diversity. To address this issue, various approaches have been proposed to improve trajectory diver-

sity. For example, DiffusionDrive[19] integrates a clustered trajectory vocabulary within an iterative refinement framework; Similarly, GoalFlow[31] predicts the top-k goal points, aggregates them and guides the flow matching process, however, it requires five sampling steps to achieve optimal performance. Despite these advancements, existing diffusion and flow matching approaches still suffer from significant limitations. One issue is the need for multiple sampling steps, which trade off inference speed and model performance. Another is their discretizations of the trajectory space, where the discretizations inherently constrain the exploration of the broader trajectory solution space and compromise their performance on test scenarios that fall outside the pre-defined anchor distribution, as shown in Fig. 2. This raises a key question: how can we effectively model the multi-modal nature of driving behaviors while maintaining strong performance **without relying on a fixed, discrete anchor vocabulary?**

To tackle the above challenges, we propose **MeanFuser**, as illustrated in Fig. 7a. First, to address the mode collapse caused by standard Gaussian noise sampling and to eliminate the dependence on a fixed discrete vocabulary, we model the noise distribution using a **Gaussian Mixture Noise (GMN)**. Unlike vocabulary-based approaches that discretize the trajectory space, GMN provides a continuous representation that covers a broader range of trajectories. Each Gaussian component captures a distinct driving pattern, effectively enhancing the model’s ability to represent multi-modal behaviors. Interestingly, we find that the

GMN also brings an additional benefit, different components naturally correspond to diverse driving styles, opening possibilities for customized autonomous driving.

Second, to accelerate sampling and eliminate the numerical errors introduced by Ordinary Differential Equation (ODE) solvers during the sampling process, we adapt “MeanFlow Identity”[9] to end-to-end planning, which directly learns the mean velocity field between the noise distribution and trajectory distribution, replacing the instantaneous velocity field used in vanilla flow matching models.

Finally, we consider a practical issue: what if all sampled proposals are suboptimal in certain cases? Our solution is to reconstruct high-quality trajectories when necessary. To achieve this, we design an **Adaptive Reconstruction Module (ARM)** that enables the model to implicitly decide via attention weights, after evaluating all proposals, whether to select an existing trajectory or to regenerate a new one. Unlike methods such as Hydra-MDP[17] and WoTE[16], which score candidate trajectories using evaluation submetrics from benchmark, ARM enhances performance while relying solely on expert trajectories.

We evaluate MeanFuser on a closed-loop benchmark NAVSIM. As shown in Fig. 7b, Under the same perception backbone, MeanFuser achieves **89.0 PDMS** on NAVSIMv1 and **89.5 EPDMS** on NAVSIMv2, surpassing previous methods. Moreover, owing to its one-step sampling design, MeanFuser achieves **59 frames per second (FPS)**, with inference speeds 5.20 \times , 2.65 \times , and 1.55 \times faster than GoalFlow, Hydra-MDP, and DiffusionDrive, respectively. Our main contributions are summarized as follows:

- We propose **MeanFuser**, the first framework that introduces the MeanFlow paradigm into end-to-end autonomous driving, achieving an effective balance between one-step sampling and planning performances.
- We propose Gaussian mixture noise (**GMN**) modeling to capture diverse driving modes without relying on fixed anchor vocabulary.
- We design an adaptive reconstruction module (**ARM**) to handle suboptimal proposals, enhancing robustness and trajectory quality in complex scenarios.
- We demonstrate that MeanFuser outperforms existing imitation learning based approaches on NAVSIM closed-loop Benchmark, achieving superior results with a rule-free and image-only design.

2. Related Work

2.1. End-to-End Autonomous Driving

End-to-end autonomous driving systems take sensory inputs and ego-vehicle states as inputs and aim to directly generate driving trajectories through neural optimization. Early works such as Transfuser[5] focused on fusing heterogeneous modalities such as camera and LiDAR, while

introducing auxiliary tasks to enhance supervision during action-space training. UniAD[12] further structured the entire framework as a planning-oriented transformer pipeline, enabling information flow across multiple specialized modules. Building on this line of research, VAD[13] replaced dense bird’s-eye-view representations with lightweight vectorized scene abstractions, which significantly improved efficiency. Its successor, VADv2[3], reformulated trajectory regression as a discrete trajectory-token selection problem, choosing the optimal trajectory from a learned vocabulary. ParaDrive[29] departed from the traditional serial end-to-end paradigm and adopted a parallel framework, allowing mapping, prediction, and planning to proceed simultaneously. Unlike the aforementioned methods, we use powerful generative models to model the trajectory distribution.

2.2. Diffusion and Flow-Based Generative Models for Trajectory Planning

Driving behaviors are inherently multimodal since in complex traffic scenarios, multiple feasible trajectories may exist. To capture this stochasticity, recent works adopt diffusion[10, 24, 25] or flow matching[20, 21] generative paradigms, training with noise injection and denoising inference to sample diverse yet plausible trajectories[19, 27, 31]. MotionDiffuser[14] was among the first to introduce diffusion-based trajectory generation in autonomous driving. Later, Diffusion-ES[32] refined the generated trajectories through iterative optimization that alternates between generation and evaluation. Diffusion Planner[37] incorporated scene context through carefully designed conditioning mechanisms that effectively guided the diffusion process. Moreover, DiffusionDrive[19] introduced noise perturbations to clustered trajectory prototypes, effectively encoding prior trajectory distributions. In contrast, GoalFlow[31] employed flow matching for improved stability and utilized goal points to explicitly guide trajectory generation. We improve the model’s performance and robustness without relying on anchor-based guidance by introducing Gaussian Mixture Noise sampling and an Adaptive Reconstruction Module, while requiring only one-step sampling.

2.3. Candidate Trajectory Proposal Evaluation and Selection

Due to the complexity of driving environments, end-to-end planners often generate a set of candidate trajectory proposals followed by a selection stage. The selection mechanism can be rule-based or learning-based. For instance, SparseDrive[26] performed trajectory rollouts conditioned on environmental predictions and evaluated them using handcrafted scoring functions. Similarly, Diffusion-ES[32] applied map-based scoring rules to filter diffusion-generated trajectories. Learning-based selectors such as DiffusionDrive[19] and WoTE[16] adopt data-driven scor-

ing mechanisms. DiffusionDrive jointly learned both trajectory generation and action-value estimation within the diffusion framework, while WoTE introduced a learned world model to simulate environment dynamics and assess candidate trajectories. These approaches bridge the gap between stochastic trajectory generation and decision-level optimization. We eliminate direct trajectory evaluation by introducing the Adaptive Reconstruction Module, allowing the model to implicitly decide whether to select from the candidates or regenerate a better trajectory based on the proposed candidates.

3. Preliminary

3.1. Problem Formulation

End-to-end autonomous driving systems take raw sensor data as input and directly predict future driving trajectories. The observational information \mathcal{O}_i at time step i typically comprises multi-view camera images $\mathcal{I}_i \in \mathbb{R}^{H \times W \times C}$, ego-vehicle state information \mathcal{S}_i (including velocity, acceleration), and high-level driving commands \mathcal{C}_i . Given the observation inputs \mathcal{O}_i , the objective is to predict a future trajectory $\hat{\tau} = \{(x_i, y_i, \theta_i)\}_{i=1}^{T_f}$, where x_i, y_i, θ_i represent the position coordinates and heading angle in the ego-vehicle coordinate system at time step i , T_f denotes the planning horizon. During training, the model learns from expert demonstration trajectories τ to optimize its parameters.

3.2. Flow-Based Model

We first introduce the foundational concepts of flow matching. Standard flow matching[20] frameworks aim to construct a continuous probability path $\{z_t\}_{t \in [0,1]}$ between a simple prior distribution p_0 (e.g., Gaussian noise) and the complex data distribution p_1 , governed by the boundary conditions $z_{t=0} = p_0$ and $z_{t=1} = p_1$, z_t is called a flow. This is achieved by learning an instantaneous velocity field $v(z_t, t)$. A sample $x_0 \sim p_0$ is then transformed into a sample $x_1 \sim p_1$ by solving the ordinary differential equation:

$$\begin{cases} \frac{dz_t}{dt} = v_\theta(z_t, t) \\ z_0 = x_0. \end{cases} \quad (1)$$

However, a critical limitation persists: even if the marginal probability path z_t is linear, which often constructible as $z_t = (1-t)x_1 + tx_0$, the learned velocity field $v_\theta(z_t, t)$ is not guaranteed to produce straight trajectories for individual samples[9]. This inherent curvature forces the use of small step sizes and multiple function evaluations (NFEs) during ODE solvers to minimize discretization error, which significantly hinders sampling efficiency.

MeanFlow[9] addresses this limitation by abandoning the modeling of instantaneous velocity fields and instead directly modeling the mean velocity field $u(z_t, r, t)$, which

is defined as the total displacement between time steps t and r divided by the time interval:

$$u(z_t, r, t) \triangleq \frac{1}{t-r} \int_r^t v(z_\tau, \tau) d\tau. \quad (2)$$

By differentiating and rearranging with respect to t , one can derive the ‘‘MeanFlow Identity’’:

$$u(z_t, r, t) = v(z_t, t) - (t-r) \frac{d}{dt} u(z_t, r, t), \quad (3)$$

where the differential term can be rewritten as:

$$\frac{d}{dt} u(z_t, r, t) = v(z_t, t) \partial_z u + \partial_t u. \quad (4)$$

This identity establishes a precise relationship between the instantaneous velocity $v(z_t, t)$ and the mean velocity $u(z_t, r, t)$, enabling the development of a novel training objective that explicitly encourages straight sample trajectories. By learning the mean velocity field u directly, the model can generate high-quality samples in a single step, as the straight-line trajectory from x_0 to x_1 is given by:

$$x_1 = x_0 + 1 \cdot u_\theta(x_0, 0, 1). \quad (5)$$

The objective of the model training is to minimize the following loss function:

$$\mathcal{L}(\theta) = \mathbb{E} \|u_\theta(z_t, r, t) - \text{sg}(u_{\text{tgt}})\|_2^2. \quad (6)$$

The $\text{sg}(\cdot)$ operator refers to the stop-gradient operator, which prevents gradients from being propagated through the target u_{tgt} during backpropagation, ensuring that only the model output is updated. The target mean velocity field u_{tgt} is defined as:

$$u_{\text{tgt}} = v(z_t, t) - (t-r) (v(z_t, t) \partial_z u_\theta + \partial_t u_\theta), \quad (7)$$

where the velocity field $v(z_t, t)$ is given by $v(z_t, t) = x_0 - x_1$. During training, we compute the Jacobian-vector product (JVP) of the function $u(z_t, r, t)$ using `torch.autograd.functional.jvp`. For this, we use the tangent vector $[v, 0, 1]$, which allows us to obtain the derivatives $\partial_z u_\theta$ and $\partial_t u_\theta$.

4. Method

The overall pipeline of MeanFuser is illustrated in Fig. 3 of our model architecture, it consists of three main components: the model training, the multi-modal trajectories sample, and the adaptive reconstruction module.

4.1. Scene Context Encoder

The scene encoder consists of two components: an image encoder \mathcal{E}_I and an ego-vehicle state encoder \mathcal{E}_s , which are

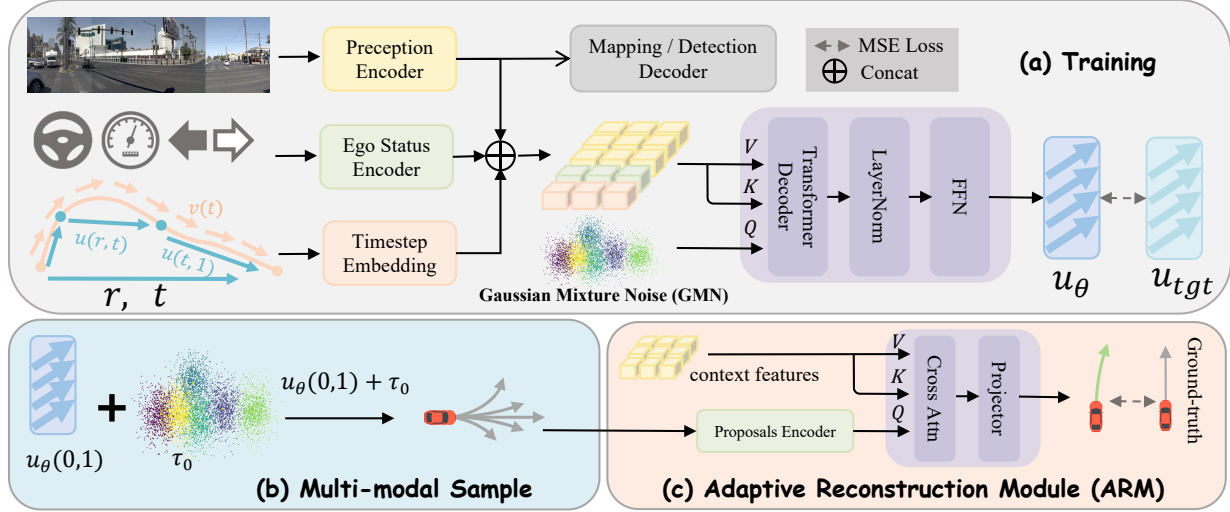


Figure 3. Overall architecture of MeanFuser. **Training:** During training, both the images and ego-vehicle states are encoded into context features, with auxiliary supervision from mapping and detection tasks. The model is conditioned on these context features to learn the average velocity field u_θ over the time interval r and t . **Multi-Modal Sample:** Noise samples are drawn from Gaussian Mixture Noise, and the one-step sampling formulation is then applied to generate diverse multi-modal trajectories. **Adaptive Reconstruction Module:** The sampled multi-modal trajectories are encoded and fused with the context features through cross-attention, after which a Projector outputs the final planning trajectory.

used to extract high-dimensional key features specific to the scene,

$$\mathbf{c}_{\text{bev}} = \mathcal{E}_I(\mathcal{I}_i), \quad \mathbf{c}_s = \mathcal{E}_s(\mathcal{S}_i, \mathcal{C}_i). \quad (8)$$

During training, an auxiliary decoder is employed to decode dynamic information of surrounding traffic participants and the lane map from \mathbf{c}_{bev} , with the corresponding loss functions \mathcal{L}_{det} and \mathcal{L}_{map} applied to supervise semantic learning and accelerate model convergence. The extracted scene features $\mathbf{c} = \{\mathbf{c}_{\text{bev}}, \mathbf{c}_s\}$ serve as scene-specific conditional inputs for multi-modal trajectories sampling.

4.2. Gaussian Mixture Noise

Unlike diffusion-based models, flow-based models do not require the prior distribution p_0 to follow standard Gaussian noise. In this work, to eliminate reliance on discrete vocabularies, we set p_0 as a Gaussian Mixture Noise distribution, guiding the model to generate multi-modal driving trajectories.

Concretely, we normalize expert demonstrations in the training set. For each trajectory τ_j , we compute

$$\Delta\tau_j = \{(\tau_j)\}_{t=1}^T - \{(\tau_j)\}_{t=0}^{T-1}. \quad (9)$$

We further compute $\Delta\tau_{\text{mean}}$, $\Delta\tau_{\text{max}}$, and $\Delta\tau_{\text{min}}$ across all

trajectories and all time steps:

$$\begin{cases} \Delta\tau_{\text{mean}} = \text{mean}_{j,t}((\Delta\tau_j)_t) \\ \Delta\tau_{\text{max}} = \max_{j,t}((\Delta\tau_j)_t) \\ \Delta\tau_{\text{min}} = \min_{j,t}((\Delta\tau_j)_t). \end{cases} \quad (10)$$

Each trajectory is then scaled as

$$\Delta\tau_j = \frac{\Delta\tau_j - \Delta\tau_{\text{mean}}}{\max(\Delta\tau_{\text{max}} - \Delta\tau_{\text{mean}}, \Delta\tau_{\text{mean}} - \Delta\tau_{\text{min}})}. \quad (11)$$

All normalized trajectories are subsequently clustered into k groups using the k-means method, representing k distinct trajectory modes. The mean and standard deviation of each cluster are then computed and used to parameterize the components of the Gaussian mixture model. The prior distribution p_0 is then defined as

$$p_0 := \sum_{k=1}^K \pi_k \mathcal{N}(\mu_k, \sigma_k^2 \cdot I), \quad (12)$$

where K denotes the number of Gaussian components, π_k represents the mixing coefficient for the k -th component, μ_k is the mean, and σ_k^2 is the variance for the k -th Gaussian component. In this work, we fix $\pi_k = 1$. Exploring how to model more optimal parameters remains an interesting direction for future research.

Table 1. **Performance on the NAVSIMv1 navtest benchmark.** ‘‘C’’ denotes camera, and ‘‘L’’ denotes LiDAR. * indicates results reported from the official papers.

Method	Venue	Input	Img. Backbone	NC↑	DAC↑	TTC↑	Comf.↑	EP↑	PDMS↑
TransFuser[5]	IEEE TPAMI	C & L	ResNet-34	97.7	92.8	92.8	100	79.2	84.0
UniAD[12]	CVPR 2023	C & L	ResNet-34	97.8	91.9	92.9	100	78.8	83.4
PARADrive[29]	CVPR 2024	C & L	ResNet-34	97.9	92.4	93.0	99.8	79.3	84.0
VADv2[3]	arXiv 2024	C & L	ResNet-34	97.2	89.1	91.6	100	76.0	80.9
Hydra-MDP[17]	arXiv 2024	C & L	ResNet-34	98.3	96.0	94.6	100	78.7	86.5
GoalFlow*[31]	CVPR 2025	C & L	ResNet-34	98.3	93.8	94.3	100	79.8	85.7
DiffusionDrive [19]	CVPR 2025	C & L	ResNet-34	98.2	96.2	94.7	100	82.2	88.1
Epona [34]	ICCV 2025	C & L	Transformer	97.9	95.1	93.8	99.9	80.4	86.2
WoTE [16]	ICCV 2025	C & L	ResNet-34	98.5	96.8	94.9	99.9	81.9	88.3
MeanFuser(Ours)	-	C-Only	ResNet-34	98.6	97.0	95.0	100	82.8	89.0

Table 2. **Performance of the NAVSIMv2 navtest benchmark.** † denotes testing with the official checkpoint

Method	NC↑	DAC↑	DDC↑	TLC↑	EP↑	TTC↑	LK↑	HC↑	EC↑	EPDMS↑
Ego Status MLP[18]	93.1	77.9	92.7	99.6	86.0	91.5	89.4	98.3	85.4	64.0
TransFuser[5]	96.9	89.9	97.8	99.7	87.1	95.4	92.7	98.3	87.2	76.7
Hydra-MDP++[15]	97.2	97.5	99.4	99.6	83.1	96.5	94.4	98.2	70.9	81.4
DriveSuprim[33]	97.5	96.5	99.4	99.6	88.4	96.6	95.5	98.3	77.0	83.1
ARTEMIS[8]	98.3	95.1	98.6	99.8	81.5	97.4	96.5	98.3	-	83.1
DiffusionDrive †[19]	98.2	96.1	99.5	99.8	87.4	97.3	96.9	98.3	87.5	88.1
MeanFuser(Ours)	98.3	97.2	99.6	99.8	87.6	97.4	97.3	98.3	88.2	89.5

Table 3. **Model parameter size, inference speed, and performance.** **Bold** and underlined values denote the best and second-best results, respectively. ‘‘Dim’’ indicates the number of hidden neurons in the model, ‘‘FPS’’ represents the median inference speed measured on a single NVIDIA H20 GPU over multiple runs, and ‘‘Plan FPS’’ refers to the inference speed of trajectory planning excluding the perception encoder.

Method	Dim	Params (M)	PDMS ↑	Plan FPS ↑	FPS ↑
TransFuser	256	55.9	84.0	3934	63
GoalFlow	256	62.3	85.7	11	10
Hydra-MDP	256	65.2	86.5	25	20
DiffusionDrive	256	60.7	<u>88.1</u>	75	39
MeanFuser	128	54.6	89.0	<u>434</u>	<u>59</u>

4.3. Multi-modal Trajectories Sample

We train a lightweight network for estimating the average velocity, $u_\theta(\tau_t, r, t | \mathbf{c})$, which maps noise sample $\tau_0 \sim p_0$ to the expert trajectory τ_1 . The noise samples are used as queries, while the specific scene information \mathbf{c} , along with the encoded time intervals r and t , are concatenated to serve as the key and value for the Transformer decoder layers. These inputs are processed through LayerNorm and a feed-forward neural network (FFN) to integrate scene-specific context. This allows the network to focus on the surround-

ing agents and lane context, ensuring that the generated trajectory is consistent with the current driving scenario. Accordingly, the loss function of the decoder can be formulated as:

$$\mathcal{L}_{flow} = \|u_\theta(\tau_t, r, t | \mathbf{c}) - \text{sg}(u_{tgt})\|_1. \quad (13)$$

During training, we select the Gaussian component nearest to the ground truth (using Euclidean distance) and compute its loss only. During model inference, we sample noise points from each Gaussian component and generate planning trajectories in parallel. Each noise point corresponds to a trajectory of a specific driving mode.

4.4. Adaptive Reconstruction Module

Model sampling generates multimodal trajectories $\{\hat{\tau}_k\}_{k=1}^K$, where K denotes the number of candidates. All candidate trajectories and c_{bev} are processed by a cross-attention layer, and the resulting representation is fed into a Projector to yield the final trajectory $\hat{\tau}$.

During training, we supervise the ARM parameters with expert demonstrations, and compute the loss as follows:

$$\mathcal{L}_\tau = \|\tau - \hat{\tau}\|_1, \quad (14)$$

where τ denotes the ground-truth expert trajectory. The model’s training does not rely on evaluation metrics from benchmark.

Table 4. **Ablation study on the impact of each module.** Base denotes the TransFuser[5] baseline. \mathcal{M}_0 replaces the decoder MLP in TransFuser with a MeanFlow model and employs a classifier to score the parallel sampled trajectory proposals. \mathcal{M}_1 and \mathcal{M}_2 further enhance \mathcal{M}_0 by introducing GMN and an ARM, respectively. \mathcal{M}_3 employs an averaging strategy across all sampled trajectories. $N_{proposals}$ denotes the number of sampled trajectory proposals; $P_{L_2>0.2}$ and $P_{L_2>0.5}$ represent the proportions of scenarios where all proposals have a minimum L_2 distance greater than 0.2 and 0.5 from the expert trajectory; and $N_{DAC=0}$ indicates the number of cases where all proposals leave the drivable area.

Model	Components	PDMS \uparrow	$N_{proposals}$	$P_{L_2>0.2}\downarrow$	$P_{L_2>0.5}\downarrow$	$N_{DAC=0}\downarrow$
-	DiffusionDrive	88.1	20	72.7%	20.0%	84
Base	TransFuser	84.0	-	-	-	-
\mathcal{M}_0	Base + vanilla MeanFlow	87.3 $+3.3$	16	92.8%	40.6%	143
\mathcal{M}_1	\mathcal{M}_0 + Guassian-mixed Noise (GMN)	88.2 $+0.9$	16	69.3%	18.5%	58
\mathcal{M}_2	\mathcal{M}_1 + Adaptive Reconstruction Module (ARM)	89.0$+0.8$	17	67.1%	16.9%	48
\mathcal{M}_3	\mathcal{M}_1 + Trajectory Proposals Averaging	71.2 -17.8	17	69.1%	18.0%	57

The total loss function is a weighted sum of the losses from Meanflow decoder, Mapping, Detection, and ARM, as follows:

$$\mathcal{L} = \lambda_1 \mathcal{L}_\tau + \lambda_2 \mathcal{L}_{flow} + \lambda_3 \mathcal{L}_{map} + \lambda_4 \mathcal{L}_{det} \quad (15)$$

The hyperparameters λ_1 , λ_2 , λ_3 and λ_4 control the relative importance of each component loss.

5. Experiments

5.1. Dataset and Metrics

NAVSIMv1: The NAVSIM dataset[7] is an end-to-end planning-oriented subset derived from the nuPlan dataset[1]. During the collection process, static scenarios and constant-speed driving scenarios were excluded, leaving behind a large set of challenging scenarios. NAVSIMv1 uses non-reactive simulations along with closed-loop evaluation metrics. The evaluation metric, **PDM Score (PMDS)**, is a weighted combination of five sub-metrics: no collisions (NC), drivable area compliance (DAC), time-to-collision (TTC), comfort (Comf.), and Ego Progress (EP). The dataset is divided into fixed sets: navtrain and navtest, which are used for training and testing, respectively.

NAVSIMv2: NAVSIMv2[28] offers more comprehensive evaluation metrics and a reactive simulation environment than NAVSIMv1, enabling performance assessment in challenging scenarios. Model performance is reflected by the **Extended PDM Score (EPDMS)**, which augments the original PDMS with additional submetrics: driving direction compliance (DDC), traffic light compliance (TLC), lane keeping (LK), history comfort (HC), and extended comfort (EC).

5.2. Implementation Detail

We apply AdamW with weight decay 0.1, using a cosine-annealed schedule that starts at 2×10^{-4} and includes a 3-epoch warm-up. The network uses a hidden dimension of

128 and emits 4-second trajectories at 2 Hz, yielding eight discrete waypoints. During both training and inference, the noise distribution is parameterized as an 8-component Gaussian mixture ($K = 8$), and we sample eight trajectories in parallel for each scene.

5.3. Main Results

As shown in Tab. 1 and Tab. 2, under a shared ResNet-34 visual backbone, MeanFuser achieves the strongest closed-loop performance on both NAVSIM-v1 and NAVSIM-v2 benchmarks using only RGB visual input (without LiDAR), outperforming all multimodal (C&L) competitors. On NAVSIMv1, MeanFuser reaches a PDMS of **89.0**, surpassing the diffusion-based DiffusionDrive by **+0.9** and the flow based GoalFlow by **+3.3**, while achieving the highest scores across all sub-metrics. On NAVSIMv2, which emphasizes generalization and reactive control, further confirms these findings. MeanFuser attains state-of-the-art performance with **EPDMS = 89.5**, showing remarkable gains on the LK and EC metrics and continuous improvement in compliance and safety indicators. Overall, these results demonstrate that explicitly modeling multimodal uncertainty in the trajectory space through the Gaussian mixture formulation, combined with adaptive trajectory reconstruction, enables MeanFuser to achieve superior driving performance under a lightweight vision-only setup while substantially enhancing safety margins and regulatory compliance.

As shown in Tab. 3, we further compare the performance and inference speed of different models. The results highlight the significant advantage of MeanFuser’s lightweight network design. MeanFuser achieves the highest PDMS of 89.0 and an impressive inference speed of 59 FPS, outperforming the Hydra-MDP model on both metrics. The one-step sampling strategy used in MeanFuser eliminates the need for time-consuming iterative sampling. Notably, when using the same perception model, MeanFuser accelerates the trajectory planning module by 39.45 \times and 5.78 \times

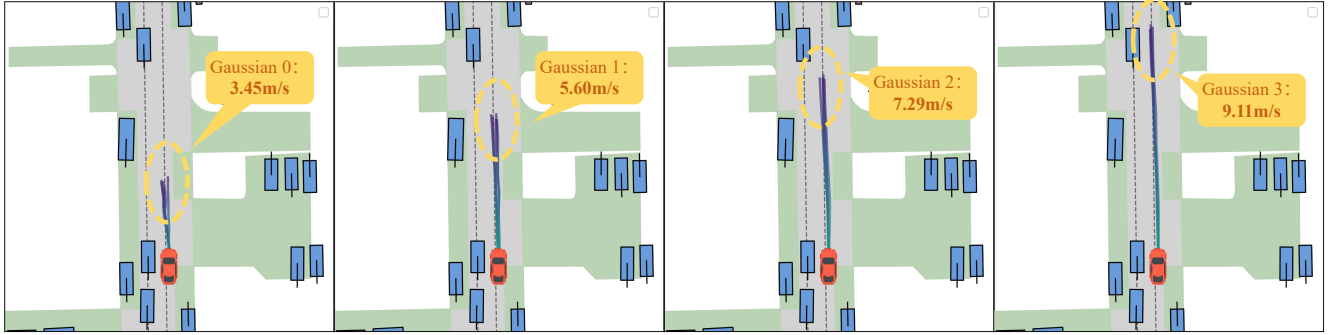


Figure 4. Visualization of sampling from different Gaussian components. Parallel sampling of trajectories from distinct Gaussian components can generate diverse driving styles, ranging from conservative to aggressive.



Figure 5. Visualization of the multimodal trajectory of the model. The left image shows expert demonstration trajectories, while the right image displays the model’s inferred strategies for maintaining a straight path and performing a left lane change, representing two different modes.

compared to GoalFlow and DiffusionDrive, respectively. This substantially improves inference efficiency, as these baseline methods are more computationally intensive due to their reliance on multiple sampling steps or complex architectures.

5.4. Ablation Studies

The ablation of each core module. Detailed results are reported in Table 4. The baseline TransFuser model employs an MLP decoder for direct trajectory planning. Based on this, \mathcal{M}_0 replaces the MLP with a context-condition MeanFlow trajectory generator, achieving a performance gain of +3.3 PDMS. Subsequently, \mathcal{M}_1 further incorporates Gaussian Mixture Noise (GMN) guidance, and \mathcal{M}_2 replaces the classifier-based scoring mechanism with the proposed Adaptive Reconstruction Module (ARM), yielding additional improvements of +0.9 PDMS and +0.8 PDMS, respectively. This culminates in a final performance of 89.0 PDMS. In contrast, \mathcal{M}_3 , which simply averages all trajectory proposals instead of utilizing ARM, suffers a significant performance drop of 17.8 PDMS. This substantial decline indicates that our sampled trajectory proposals capture diverse behaviors rather than collapsing into a single, aver-

aged mode.

To further evaluate robustness, we analyze the proportion of scenarios where all trajectory proposals deviate from the expert trajectory by more than 0.2 or 0.5 in Euclidean distance, as well as the number of cases where all proposals leave the drivable area ($DAC = 0$). Compared to DiffusionDrive, \mathcal{M}_1 successfully handles a greater number of challenging scenarios despite utilizing fewer trajectory proposals. This confirms that GMN provides broader coverage of the trajectory solution space than conventional anchor-based guidance. Furthermore, a comparison between \mathcal{M}_1 and \mathcal{M}_0 reveals 85 additional $DAC = 0$ cases for the latter, demonstrating that the GMN sampling method captures a richer diversity of driving strategies compared to standard Gaussian noise sampling, thereby being able to cover the optimal driving behavior. Finally, by integrating the trajectory regeneration capability of ARM, \mathcal{M}_2 reduces the number of $DAC = 0$ cases to 48 from 58, underscoring ARM’s effectiveness in generating higher-quality trajectories when all initially sampled proposals are suboptimal.

5.5. Qualitative Analysis

Multi-modal trajectory proposals. As shown in Fig. 5, we demonstrate the model’s multi-modal capability in a specific driving scenario, where it samples both a lane-keeping strategy that closely follows the expert demonstration and an alternative strategy that performs a left-lane change.

Differentiated driving styles. As shown in Fig. 4, we visualize 8 trajectory proposals in a specific scenario. All 8 trajectories in each image are sampled from the same Gaussian component. As the mean of the Gaussian component increases, the model’s planned trajectory speed rises progressively from 3.45 m/s to 9.11 m/s, reflecting a shift from conservative to aggressive driving behavior. This demonstrates that the Gaussian Mixture Noise sampling approach

enables the modeling of differentiated driving styles.

6. Conclusion

This paper presents a novel end-to-end autonomous driving planning framework MeanFuser that overcomes the limitations of discrete vocabulary dependency and achieves an effective balance between one-step sampling and planning performances. We introduce three technical contributions: Gaussian mixture noise, the “MeanFlow identity”, and an adaptive reconstruction module. We further show its effectiveness and provide extensive analysis of the framework’s planning performance, computational efficiency, and trajectory diversity.

References

- [1] Holger Caesar, Juraj Kabzan, Kok Seang Tan, Whye Kit Fong, Eric Wolff, Alex Lang, Luke Fletcher, Oscar Beijbom, and Sammy Omari. nuplan: A closed-loop ml-based planning benchmark for autonomous vehicles. *arXiv preprint arXiv:2106.11810*, 2021. 7
- [2] Li Chen, Penghao Wu, Kashyap Chitta, Bernhard Jaeger, Andreas Geiger, and Hongyang Li. End-to-end autonomous driving: Challenges and frontiers. *IEEE Transactions on Pattern Analysis and Machine Intelligence*, 2024. 2
- [3] Shaoyu Chen, Bo Jiang, Hao Gao, Bencheng Liao, Qing Xu, Qian Zhang, Chang Huang, Wenyu Liu, and Xinggang Wang. Vadv2: End-to-end vectorized autonomous driving via probabilistic planning. *arXiv preprint arXiv:2402.13243*, 2024. 2, 3, 6
- [4] Cheng Chi, Zhenjia Xu, Siyuan Feng, Eric Cousineau, Yilun Du, Benjamin Burchfiel, Russ Tedrake, and Shuran Song. Diffusion policy: Visuomotor policy learning via action diffusion. *The International Journal of Robotics Research*, page 02783649241273668, 2023. 2
- [5] Kashyap Chitta, Aditya Prakash, Bernhard Jaeger, Zehao Yu, Katrin Renz, and Andreas Geiger. Transfuser: Imitation with transformer-based sensor fusion for autonomous driving. *IEEE transactions on pattern analysis and machine intelligence*, 45(11):12878–12895, 2022. 2, 3, 6, 7, 1
- [6] Hyungjin Chung, Jeongsol Kim, Geon Yeong Park, Hyelin Nam, and Jong Chul Ye. Cfg++: Manifold-constrained classifier free guidance for diffusion models. *arXiv preprint arXiv:2406.08070*, 2024. 2
- [7] Daniel Dauner, Marcel Hallgarten, Tianyu Li, Xinshuo Weng, Zhiyu Huang, Zetong Yang, Hongyang Li, Igor Gilitschenski, Boris Ivanovic, Marco Pavone, et al. Navsim: Data-driven non-reactive autonomous vehicle simulation and benchmarking. *Advances in Neural Information Processing Systems*, 37:28706–28719, 2024. 7
- [8] Renju Feng, Ning Xi, Duanfeng Chu, Rukang Wang, Zejian Deng, Anzheng Wang, Liping Lu, Jinxiang Wang, and Yanjun Huang. Artemis: Autoregressive end-to-end trajectory planning with mixture of experts for autonomous driving. *arXiv preprint arXiv:2504.19580*, 2025. 6
- [9] Zhengyang Geng, Mingyang Deng, Xingjian Bai, J Zico Kolter, and Kaiming He. Mean flows for one-step generative modeling. *arXiv preprint arXiv:2505.13447*, 2025. 2, 3, 4
- [10] Jonathan Ho, Ajay Jain, and Pieter Abbeel. Denoising diffusion probabilistic models. *Advances in neural information processing systems*, 33:6840–6851, 2020. 2, 3
- [11] Shengchao Hu, Li Chen, Penghao Wu, Hongyang Li, Junchi Yan, and Dacheng Tao. St-p3: End-to-end vision-based autonomous driving via spatial-temporal feature learning. In *European Conference on Computer Vision*, pages 533–549. Springer, 2022. 2
- [12] Yihan Hu, Jiazhi Yang, Li Chen, Keyu Li, Chonghao Sima, Xizhou Zhu, Siqi Chai, Senyao Du, Tianwei Lin, Wenhai Wang, et al. Planning-oriented autonomous driving. In *Proceedings of the IEEE/CVF conference on computer vision and pattern recognition*, pages 17853–17862, 2023. 2, 3, 6
- [13] Bo Jiang, Shaoyu Chen, Qing Xu, Bencheng Liao, Jiajie Chen, Helong Zhou, Qian Zhang, Wenyu Liu, Chang Huang, and Xinggang Wang. Vad: Vectorized scene representation for efficient autonomous driving. In *Proceedings of the IEEE/CVF International Conference on Computer Vision*, pages 8340–8350, 2023. 2, 3
- [14] Chiyu Max Jiang, Andre Cornman, Cheolho Park, Benjamin Sapp, Yin Zhou, and Dragomir Anguelov. Motiondiffuser: Controllable multi-agent motion prediction using diffusion. In *2023 IEEE/CVF Conference on Computer Vision and Pattern Recognition (CVPR)*, pages 9644–9653. IEEE Computer Society, 2023. 3
- [15] Kailin Li, Zhenxin Li, Shiyi Lan, Yuan Xie, Zhizhong Zhang, Jiayi Liu, Zuxuan Wu, Zhiding Yu, and Jose M Alvarez. Hydra-mdp++: Advancing end-to-end driving via expert-guided hydra-distillation. *arXiv preprint arXiv:2503.12820*, 2025. 6
- [16] Yingyan Li, Yuqi Wang, Yang Liu, Jiawei He, Lue Fan, and Zhaoxiang Zhang. End-to-end driving with online trajectory evaluation via bev world model. In *International Conference on Computer Vision*, 2025. 3, 6
- [17] Zhenxin Li, Kailin Li, Shihao Wang, Shiyi Lan, Zhiding Yu, Yishen Ji, Zhiqi Li, Ziyue Zhu, Jan Kautz, Zuxuan Wu, et al. Hydra-mdp: End-to-end multimodal planning with multi-target hydra-distillation. *arXiv preprint arXiv:2406.06978*, 2024. 1, 2, 3, 6
- [18] Zhiqi Li, Zhiding Yu, Shiyi Lan, Jiahan Li, Jan Kautz, Tong Lu, and Jose M Alvarez. Is ego status all you need for open-loop end-to-end autonomous driving? In *2024 IEEE/CVF Conference on Computer Vision and Pattern Recognition (CVPR)*, pages 14864–14873. IEEE Computer Society, 2024. 6
- [19] Bencheng Liao, Shaoyu Chen, Haoran Yin, Bo Jiang, Cheng Wang, Sixu Yan, Xinbang Zhang, Xiangyu Li, Ying Zhang, Qian Zhang, et al. Diffusiondrive: Truncated diffusion model for end-to-end autonomous driving. In *Proceedings of the Computer Vision and Pattern Recognition Conference*, pages 12037–12047, 2025. 1, 2, 3, 6
- [20] Yaron Lipman, Ricky TQ Chen, Heli Ben-Hamu, Maximilian Nickel, and Matt Le. Flow matching for generative modeling. *arXiv preprint arXiv:2210.02747*, 2022. 2, 3, 4

- [21] Xingchao Liu, Chengyue Gong, and Qiang Liu. Flow straight and fast: Learning to generate and transfer data with rectified flow. *arXiv preprint arXiv:2209.03003*, 2022. 2, 3
- [22] Xueyi Liu, Zuodong Zhong, Qichao Zhang, Yuxin Guo, Yupeng Zheng, Junli Wang, Dongbin Zhao, Yun-Fu Liu, Zhiguo Su, Yinfeng Gao, et al. Reasonplan: Unified scene prediction and decision reasoning for closed-loop autonomous driving. In *Conference on Robot Learning*, pages 3051–3068. PMLR, 2025. 2
- [23] Juyi Sheng, Ziyi Wang, Peiming Li, and Mengyuan Liu. Mp1: Meanflow tames policy learning in 1-step for robotic manipulation. *arXiv preprint arXiv:2507.10543*, 2025. 2
- [24] Jiaming Song, Chenlin Meng, and Stefano Ermon. Denoising diffusion implicit models. *arXiv preprint arXiv:2010.02502*, 2020. 2, 3
- [25] Yang Song, Jascha Sohl-Dickstein, Diederik P Kingma, Abhishek Kumar, Stefano Ermon, and Ben Poole. Score-based generative modeling through stochastic differential equations. *arXiv preprint arXiv:2011.13456*, 2020. 2, 3
- [26] Wenchao Sun, Xuewu Lin, Yining Shi, Chuang Zhang, Hao-ran Wu, and Sifa Zheng. Sparsedrive: End-to-end autonomous driving via sparse scene representation. In *2025 IEEE International Conference on Robotics and Automation (ICRA)*, pages 8795–8801. IEEE, 2025. 3
- [27] Junli Wang and Qichao Zhang. Consistencydrive: Efficient end-to-end autonomous driving with consistency models. In *2025 10th International Conference on Control, Robotics and Cybernetics (CRC)*, pages 57–62. IEEE, 2025. 3
- [28] Cao Wei, Hallgarten Marcel, et al. Pseudo-simulation for autonomous driving. *arXiv preprint arXiv:2506.04218*, 2025. 7
- [29] Xinshuo Weng, Boris Ivanovic, Yan Wang, Yue Wang, and Marco Pavone. Para-drive: Parallelized architecture for real-time autonomous driving. In *Proceedings of the IEEE/CVF Conference on Computer Vision and Pattern Recognition*, pages 15449–15458, 2024. 3, 6
- [30] Penghao Wu, Xiaosong Jia, Li Chen, Junchi Yan, Hongyang Li, and Yu Qiao. Trajectory-guided control prediction for end-to-end autonomous driving: A simple yet strong baseline. *Advances in Neural Information Processing Systems*, 35:6119–6132, 2022. 2
- [31] Zebin Xing, Xingyu Zhang, et al. Goalflow: Goal-driven flow matching for multimodal trajectories generation in end-to-end autonomous driving. In *Proceedings of the Computer Vision and Pattern Recognition Conference*, pages 1602–1611, 2025. 1, 2, 3, 6
- [32] Brian Yang, Huangyuan Su, Nikolaos Gkanatsios, Tsung-Wei Ke, Ayush Jain, Jeff Schneider, and Katerina Fragkiadaki. Diffusion-es: Gradient-free planning with diffusion for autonomous and instruction-guided driving. In *2024 IEEE/CVF Conference on Computer Vision and Pattern Recognition (CVPR)*, pages 15342–15353. IEEE Computer Society, 2024. 3
- [33] Wenhao Yao, Zhenxin Li, Shiyi Lan, Zi Wang, Xinglong Sun, Jose M Alvarez, and Zuxuan Wu. Drivesuprim: Towards precise trajectory selection for end-to-end planning. *arXiv preprint arXiv:2506.06659*, 2025. 6
- [34] Kaiwen Zhang, Zhenyu Tang, Xiaotao Hu, , et al. Epona: Autoregressive diffusion world model for autonomous driving. In *International Conference on Computer Vision*, 2025. 6
- [35] Qinglun Zhang, Zhen Liu, Haoqiang Fan, Guanghui Liu, Bing Zeng, and Shuaicheng Liu. Flowpolicy: Enabling fast and robust 3d flow-based policy via consistency flow matching for robot manipulation. In *Proceedings of the AAAI Conference on Artificial Intelligence*, pages 14754–14762, 2025. 2
- [36] Wei Zhang, Pengfei Li, Junli Wang, Bingchuan Sun, Qihao Jin, Guangjun Bao, Shibo Rui, Yang Yu, Wencao Ding, Peng Li, et al. Dual-aeb: Synergizing rule-based and multimodal large language models for effective emergency braking. In *2025 IEEE International Conference on Robotics and Automation (ICRA)*, pages 14888–14895. IEEE, 2025. 2
- [37] Yinan Zheng, Ruiming Liang, Kexin ZHENG, Jinliang Zheng, Liyuan Mao, Jianxiong Li, Weihao Gu, Rui Ai, Shengbo Eben Li, Xianyuan Zhan, et al. Diffusion-based planning for autonomous driving with flexible guidance. In *The Thirteenth International Conference on Learning Representations*. 3

MeanFuser: Fast One-Step Multi-Modal Trajectory Generation and Adaptive Reconstruction via MeanFlow for End-to-End Autonomous Driving

Supplementary Material

7. CARLA Longest6 Benchmark

CARLA Longest6 Benchmark: The CARLA Longest6 Benchmark, introduced by TransFuser[5], is designed to reduce computational resource consumption and testing time while ensuring a balanced distribution of routes across six towns, with six test routes selected from each town, resulting in a total of 36 routes averaging 1500 meters in length. The benchmark incorporates six distinct weather conditions and six different times of day, and its evaluation metric is the Driving Score (DS), computed as a weighted average of Route Completion (RC) penalized by the Infraction Score (IS).

Table 5. **Longest6 Benchmark Results.** We show the mean and std for all metrics (RC: Route Completion, IS: Infraction Score, DS: Driving Score).

Method	RC \uparrow	IS \uparrow	DS \uparrow
Latent TransFuser[5]	95.18 ± 0.45	0.38 ± 0.05	37.31 ± 5.35
TransFuser[5]	93.38 ± 1.20	0.50 ± 0.06	47.30 ± 5.72
DiffusionDrive[19]	94.16 ± 1.46	0.69 ± 0.02	64.27 ± 2.43
MeanFuser (Ours)	94.65 ± 1.32	0.73 ± 0.05	70.08 ± 3.20

To comprehensively evaluate model performance, we validate our approach on the CARLA Longest6 closed-loop benchmark. As shown in Tab. 5, we conduct three runs for each route to compute the mean and standard deviation. Experimental results demonstrate that the model achieves a Driving Score (DS) that surpasses the unimodal trajectory method TransFuser by 22.78 and outperforms the multi-modal method DiffusionDrive by 5.81, confirming its effectiveness and robustness in closed-loop testing. In Fig. 6, we visualize the planning outcomes of our model across diverse scenarios under both daytime and nighttime conditions.

8. Further Ablation Study

The ablation of the number of Gaussian components. As shown in Tab. 6, we present the performance of the model with different numbers of Gaussian components. The model achieves optimal performance with eight Gaussian components. Adding more components beyond this point does not improve results and may even cause a slight decrease in performance. This indicates that eight components provide sufficient capacity to model the trajectory distribution. Further increases lead to each component becoming data-

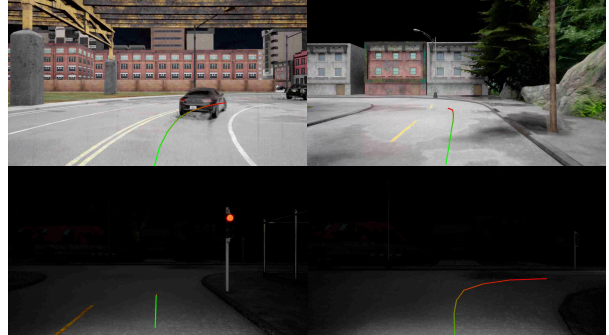


Figure 6. **Visualization on the CARLA Longest6 benchmark.** The two images in the upper row and the two in the lower row showcase the planning outcomes, depicting daytime and nighttime conditions, respectively.

Table 6. **Number of Gaussian components and model performance.** $N_{gaussian}$ denotes the number of Gaussian components in the Gaussian Mixture Noise distribution.

$N_{gaussian}$	NC \uparrow	DAC \uparrow	TTC \uparrow	Conf. \uparrow	EP \uparrow	PDMS \uparrow
2	98.1	96.9	94.0	100	81.8	88.4 -0.5
8	98.6	97.0	95.0	100	82.8	89.0
16	98.1	97.3	93.8	99.9	83.3	88.8 -0.2
32	98.0	97.0	94.3	99.9	82.8	88.5 -0.5

starved, preventing the model from adequately learning the velocity field and resulting in unreliable velocity predictions.

Table 7. **Comparison of the GMN Generation Methods.**

Method	NC \uparrow	DAC \uparrow	TTC \uparrow	Conf. \uparrow	EP \uparrow	PDMS \uparrow
Data Clustering	98.6	97.0	95.0	100	82.8	89.0
Manual Design	98.2	97.0	94.1	100	83.0	88.6 -0.4

The ablation study of Gaussian Mixture Noise generation. To investigate the dependence of model performance on Gaussian Mixture Noise (GMN) generation strategies, we conduct a comprehensive ablation study. As summarized in Tab. 7, we quantitatively compare two GMN construction methods: one derived from clustering expert tra-

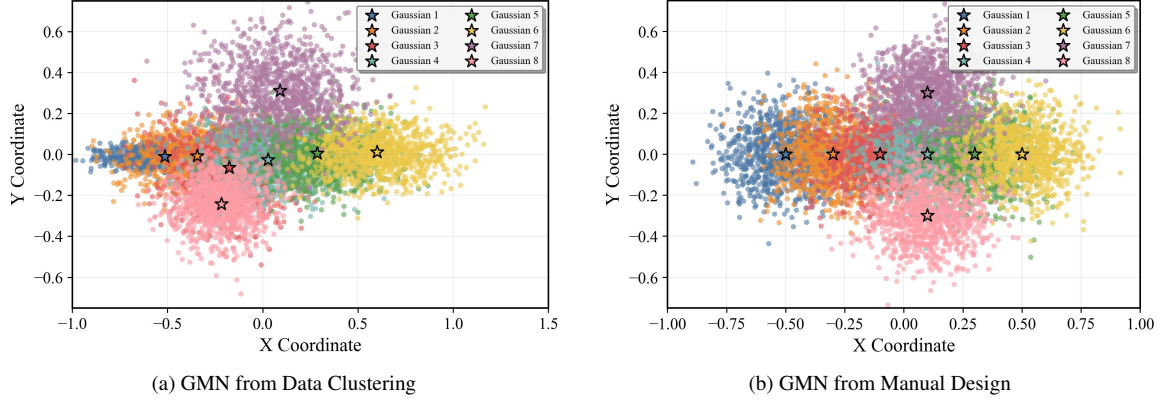


Figure 7. **Visualization of alternative approaches for generating Gaussian Mixture Noise (GMN).** (a) Mean and standard deviation are derived from clustered expert demonstrations in the training set. (b) Mean and standard deviation are obtained through manually design.

jectories in the navtrain dataset (detailed in Section 4.2), and the other manually designed. In our manual design approach, the mean of each Gaussian component is determined by simple heuristic rules while standard deviations are set to a unified fixed value. Experimental results demonstrate that when using manually designed GMN, model performance decreases by only 0.45% compared to that of the data-driven clustering approach. In contrast, the extreme case where all Gaussian components follow standard normal distributions leads to significant performance degradation. This confirms that our model’s effectiveness does not rely on specific fixed datasets. Visual comparisons of the GMN generated by both methods are presented in Fig. 7.

Table 8. **Comparison of multimodality and performance.** (GMN: Gaussian Mixture Noise. K : number of multimodal trajectories; \mathcal{D} : multimodality metric.)

Method	GMN	K	PDMS \uparrow	\mathcal{D} \uparrow	\mathcal{M}_{DP} \uparrow
TransFuser	-	8	94.0	0.0	-
MeanFuser	\times	8	88.3	0.25	22.07
MeanFuser	\checkmark	8	89.0	0.30	26.70 _{+20.84%}

The ablation study of Multi-modal planning performance.

We employ a mean Intersection-over-Union (mIoU)-based metric \mathcal{D} to quantify the multimodality of planning outcomes. For a set of K trajectories $\{\tau_k\}_{k=1}^K$, the metric is defined as:

$$\mathcal{D} = 1 - \frac{1}{T_f} \sum_{i=1}^{T_f} \frac{\bigcap_{k=1}^K \text{Area}(\hat{\tau}_{ki})}{\bigcup_{k=1}^K \text{Area}(\hat{\tau}_{ki})}, \quad (16)$$

where T_f denotes the prediction horizon, $\hat{\tau}_{ki}$ represents the bounding box of the k -th trajectory at timestep i , and the op-

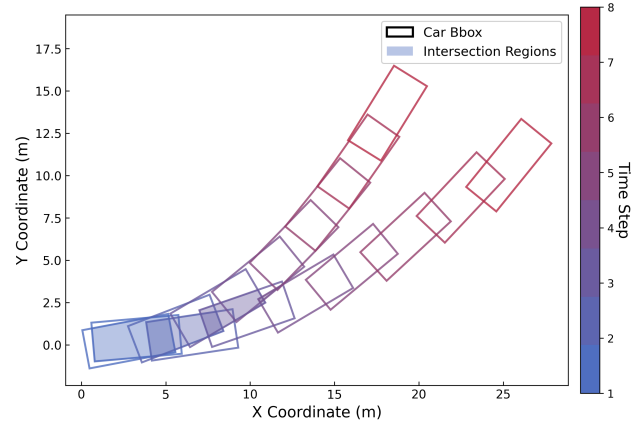


Figure 8. Visualization of the intersection and union dynamics of bounding boxes (Car Bbox) for ego trajectories across different timesteps.

erators \cap and \cup calculate the intersection and union of areas across all K trajectories at each timestep i , respectively. A higher value of \mathcal{D} indicates greater diversity among the predicted trajectories. For an intuitive understanding, Fig. 8 visualizes the bounding boxes at different timesteps along with their intersections.

To ensure that the observed diversity does not stem from model error, such as trajectory divergence, we introduce the composite metric:

$$\mathcal{M}_{DP} = \mathcal{D} \times PDMS, \quad (17)$$

which provides a unified measure that considers both planning performance and trajectory diversity.

The ablation studies in Tab. 8 demonstrate that the GMN not only enhances the primary performance metric (PDMS) but also significantly increases the diversity (\mathcal{D}) of the generated trajectory proposals, resulting in a 20.84% improvement in the comprehensive evaluation metric \mathcal{M}_{DP} .